Research Paper

Texture Evolution of Magnesium Alloy AZ31B Subjected to Severe Plastic Deformation

Karol FRYDRYCH

Institute of Fundamental Technological Research
Polish Academy of Sciences

Pawińskiego 5B, 02-106 Warsaw, Poland
e-mail: kfryd@ippt.pan.pl
ORCID: 0000-0002-9040-1523

The paper presents the simulations of texture evolution of the AZ31B Mg alloy subjected to equal channel angular pressing (ECAP) and rotary swaging (RS) processes. It is shown that using the crystal plasticity (CP) parameters obtained by curve fitting conducted on simple mechanical tests with the aid of the evolutionary algorithm, it is possible to correctly predict the texture evolution in both processes. The influence of the initial texture as well as the CP parameters is discussed.

Key words: crystal plasticity; rotary swaging; ECAP; magnesium alloys; AZ31B; severe plastic deformation.

1. Introduction

Magnesium (Mg) and its alloys are of interest for contemporary industry due to their high specific strength. For instance, application of such materials leads to lowering the mass of the vehicle thus decreasing the fuel consumption. However, one of the main drawbacks to these materials is their low ductility. Therefore, it is crucial to find a way for its improvement without decreasing the strength. The properties of the materials can be improved by changing their microstructure. For example, Fu *et al.* [1] managed to obtain simultaneously high strength and ductility in Mg-Li alloy. The authors used ultrahigh pressure combined with high temperature to obtain densely hierarchical double contraction nanotwins. Among the possible methods useful for improvements of properties by modification of microstructure are severe plastic deformation (SPD) processes.

The crystal plasticity (CP) theory directly accounts for dislocation glide on slip systems although in a continuous fashion as opposed to discrete dislocation dynamics or even lower scale models. The twinning phenomenon is treated as

a pseudo slip. Magnesium and its alloys possess hexagonal close packed (HCP) lattice. Due to a higher number of possible slip and twinning systems, simulations of such materials are typically more challenging than for highly symmetric face centered cubic (FCC) materials such as copper or aluminum. Nevertheless, there have been so far many efforts to simulate the response of such materials using the CP theory, see [2–8]. From the computational point of view, the CP simulations of SPD processes are even more demanding due to extremely large deformations present in such processes.

One example of severe plastic deformation (SPD) is the equal channel angular pressing (ECAP) process [9, 10], which consists of pressing a billet of material through an angular channel. Deformation in a single pass can be approximated as a simple shear, see Fig. 1. Usually, to obtain significant grain refinement and high strength of the material, the process is conducted multiple times. However, even a single pass introduces large amount of strain and leads to considerable evolution of texture.
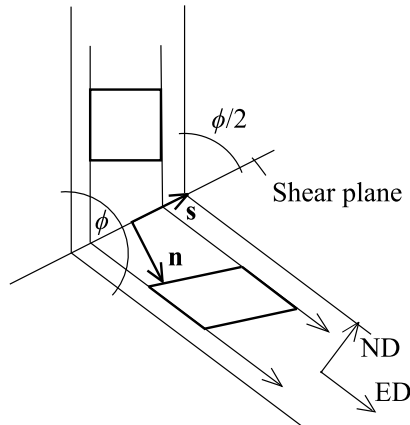

Fig. 1. Schematic showing the simple shear as applied in ECAP [10].

The evolution of microstructure of Mg and its alloys subjected to ECAP was experimentally investigated in a number of papers, see [11–25]. The CP simulations of microstructure response were also carried out and presented in some papers [12, 16, 17, 19, 21, 26], in every case using the visco-plastic self-consistent (VPSC) model [27–29]. The reason for using the VPSC model for coupling the responses of individual grains is its robustness when it comes to anisotropic plasticity and large deformations. Simulating the ECAP process for HCP material using, e.g., the crystal plasticity finite element method (CPFEM), see [30, 31] would be much more challenging, primarily due to large element distortions. Although some promising ideas of using the remeshing and solution mapping in the Lagrangian approach were discussed [31] and solving the problem

in the Eulerian setting in [32], their application to HCP materials was not carried out yet. Thus, in line with the literature, the simulations presented in this paper have also been performed using the VPSC approach.

The rotary swaging (RS) is a forming process similar to conventional swaging, but where the billet is uniformly compressed along its periphery, see [33, 34]. So far, there have been some experimental investigation of microstructure evolution in Mg and its alloys subjected to RS. KNAUER *et al.* [35] investigated the grain refinement and texture evolution in AZ31 Mg alloy subjected to room-temperature rotary swaging. Microstructure and mechanical properties of pure Mg subjected to rotary swaging were investigated in [36]. The properties of Mg alloy WE43 subjected to RS were investigated in [37]. Although the cited studies present valuable experimental results, no comprehensive micromechanical modeling of microstructure evolution of Mg and its alloys subjected to RS was presented. One of the aims of this paper is to fill this gap.

After this introductory section, the modeling framework is presented. Section 3 presents the results of simulations of ECAP and RS processes. Finally, Sec. 4 provides the discussion, and Sec. 5 presents a summary and conclusions.

2. Modeling

The well-known visco-plastic self-consistent code [28, 29, 38] was applied in this research. The code was additionally supplied with the probabilistic twin volume consistent (PTVC) reorientation model and hardening laws accounting for slip-slip, slip-twin, twin-slip and twin-twin interactions [39, 40]. Similar model was already applied e.g. in [6, 7, 41, 42]. For the sake of conciseness, the model shall be briefly outlined in the following.

In the CP theory, the velocity gradient is usually additively decomposed into elastic (index e) and plastic (index p) parts:

$$(2.1) \qquad \mathbf{l} = \mathbf{l}^e + \mathbf{l}^p = \boldsymbol{\omega}^e + \mathbf{l}^p.$$

Since the elastic stretching is very small, it is neglected and thus the elastic part of the velocity gradient is equal to the elastic spin $\boldsymbol{\omega}^e$. The Schmid tensor $\mathbf{m}^r \otimes \mathbf{n}^r$ for a given system r is used to calculate the plastic part of the velocity gradient:

$$(2.2) \qquad \mathbf{l}^p = \sum_{r=1}^{2M+N} \dot{\gamma}^r \mathbf{m}^r \otimes \mathbf{n}^r,$$

where M is the number of slip systems and N is the number of twinning systems. The rate of shearing on a given system is equal to [43]:

$$(2.3) \qquad \dot{\gamma}^r = \dot{\gamma}_0 \left(\frac{\tau^r}{\tau_c^r} \right)^n.$$

In this equation, n is the power-law exponent and $\dot{\gamma}_0$ is the reference value of the shear rate equal to 0.001. The resolved shear stress (RSS) $\tau^r = \langle \mathbf{m}^r \cdot \boldsymbol{\sigma} \cdot \mathbf{n}^r \rangle$ ($\langle \cdot \rangle \equiv \frac{1}{2}((\cdot) + |\cdot|)$) on system r is characterized using its plane normal $\mathbf{n}^r$ and direction $\mathbf{m}^r$. The evolution of the RSS's critical value – the critical resolved shear stress (CRRS) is described using the hardening law [39, 40].

Following [44, 45], twinning is treated as pseudo-slip. The volume fraction of twinning is related to the rate of shearing on the given twinning system by:

$$(2.4) \qquad \dot{f}^r = \frac{\dot{\gamma}^r}{\gamma^{TW}},$$

where γ^{TW} is the characteristic twin shear. The PTVC scheme [39, 40] ensures that this volume fraction is consistent with the fraction of reoriented grains.

The CRSSs of slip and twinning systems evolve with the accumulated slip and twin volume fraction according to the laws developed in [39, 40]. The CRSS of slip systems due to slip and twinning is governed by the equation:

$$(2.5) \qquad \dot{\tau}^r_c = \dot{\tau}^{r+M}_c = H^r_{(ss)} \sum_{q=1}^{M} h^{(ss)}_{rq} \dot{\bar{\gamma}}^q + H^r_{(st)} \sum_{q=2M+1}^{2M+N} h^{(st)}_{rq} \dot{\gamma}^q,$$

where $\dot{\bar{\gamma}}^q = \dot{\gamma}^q + \dot{\gamma}^{q+M}$. The submatrices $h^{(\alpha\beta)}_{rq} = q^{(\alpha\beta)} + (1 - q^{(\alpha\beta)})|\mathbf{n}^r \cdot \mathbf{n}^q|$, where $q^{(\alpha\beta)}$ describe the latent hardening on a given system α due to activity on system β. The coplanarity of systems is taken into account through the term $|\mathbf{n}^r \cdot \mathbf{n}^q|$. The hardening moduli $H^r_{(ss)}$ (hardening of slip due to slip) and $H^r_{(st)}$ (hardening of slip due to twinning) are defined as follows:

$$(2.6) \qquad H^r_{(ss)} = h^{ss}_0 \left(1 - \frac{\tau^r_c}{\tau^r_{sat}}\right)^\beta, \qquad H^r_{(st)} = \frac{h^{st}_0}{\tau^r_c} \left(\frac{f^{TW}}{f^{st}_{sat} - f^{TW}}\right).$$

In the preceding equation, f^{TW} is the total volume fraction of twins while $h^{\alpha s}_0, \beta, \tau^r_{sat}$, and $f^{\alpha t}_{sat}$ are material hardening parameters. The hardening laws of twinning systems due to slip and twinning activity are analogous (see e.g. [7] for details). In addition, the parameter μ is used in the formulation. Its function is to multiply the CRSSs of the systems in twin-reoriented grains which accounts for the fact, that twins have different mechanical properties than the matrix, see [46].

3. Results

3.1. ECAP

The simulation of one pass through an ECAP channel was simulated and compared to experimental data available in [21]. The experiment was performed

in room temperature. Five sheets were stacked to make the square cross-section, see Fig. 2a. The material used for creating the sample was obtained using the twin roll casting technique. Figure 2b shows the fracture of the material reported in the cited paper. The authors concluded that material was not subjected to simple shear on one shear plane being the bisector of the channel angle, but rather was sheared on two planes. Thus, instead of simulating single ECAP pass with channel angle $\phi = 90°$, two passes of ECAP with channel angle $\phi = 135°$ were modelled. Here, the same approach is adopted. Vectors $\mathbf{n}$ and $\mathbf{s}$ describing the planes of simple shear for two parts of the ECAP pass are as follows:

$$
\begin{aligned}
\mathbf{n}^{(1)} &= (\cos\phi/2, 0, -\sin\phi/2), & \mathbf{s}^{(1)} &= (\sin\phi/2, 0, \cos\phi/2), \\
\mathbf{n}^{(2)} &= (\sin\phi/2, 0, -\cos\phi/2), & \mathbf{s}^{(2)} &= (\cos\phi/2, 0, \sin\phi/2).
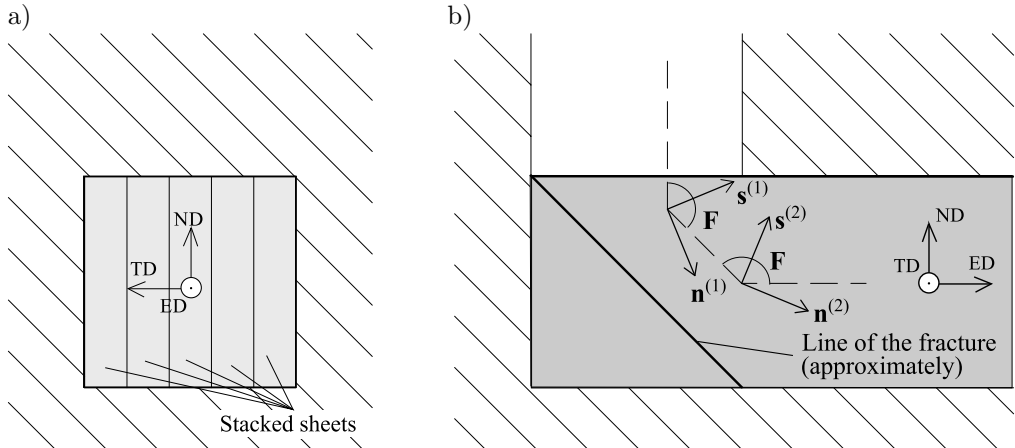\end{aligned}
$$
(3.1)

FIG. 2. The schematic showing: a) the stacking of sheets in the channel, b) the fracture of the material. The figure also shows the vectors describing the direction and plane of shearing in two simple shear used for modeling the material's deformation.

Since in [21] the experiment was conducted on AZ31B sheets, the set of the optimized CP model parameters is taken from [8], where it was established by fitting the stress-strain curves of AZ31B sheets subjected to tension and compression using the evolutionary algorithm. For the reader's convenience, the parameters are given in Table 1.

Figure 3 shows slip and twinning system activities obtained in the simulation of the ECAP process using the VPSC model. The first simple shear is dominated by the activity of basal slip. One can then easily notice sudden change connected with changing the direction of shearing. The second-order pyramidal $\langle c + a \rangle$ slip is the most active one at the beginning of the second simple shear, and afterward

Table 1. The parameters of the hardening model for AZ31B sheets [8].

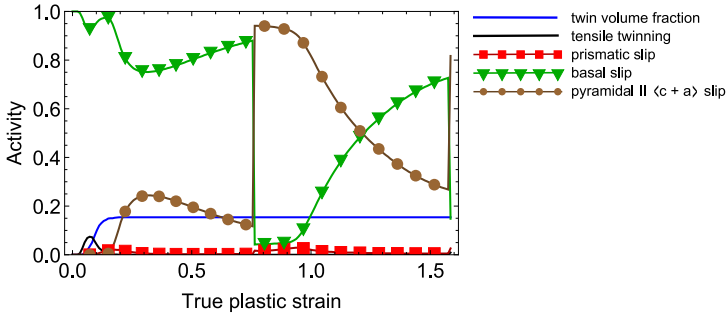| System | Interaction | τ_{c0} [MPa] | h_0 [MPa] | β | τ_{sat}/f_{sat} [MPa]/− | μ − | q | | |
---	---	---	---	---	---	---	prism.	basal twin	pyr. II
prism.	slip-slip	67.11	638.5	1.0	168.02	0.77	1.4	1.4	1.4
	slip-twin	—	1.04	—	0.75	—		1.19	
basal	slip-slip	6.76	115.78	1.0	103.15	0.8	1.4	1.4	1.4
	slip-twin	—	1.14	—	1.49	—		1.19	
pyr. II	slip-slip	85.87	1303.56	1.0	117.22	1.5	1.4	1.4	1.4
	slip-twin	—	1.02	—	0.67	—		1.19	
twin	twin-slip	—	44.25	1.0	0.0	—	1.19	1.19	1.19
	twin-twin	35.86	0.94	—	0.87	0.83		1.19	

FIG. 3. Slip and twinning system activities in the simulation of one ECAP pass.

it is gradually replaced by basal slip. Twinning is active at the beginning of the process leading to the reorientation of about 15% of grains.

Figure 4 shows pole figures for the texture: (a) initially supplied in the simulation, (b) after one ECAP pass. The initial texture is generated so that it is as similar as possible to the experimental one, see Fig. 2a in [21]. In the simulation of one ECAP pass, a similar texture to the experimental one is obtained, though some differences are present too, see Fig. 4b and Fig. 2b in the cited paper. Experimental {0001} pole figure can be characterized by one broad fiber, whereas the simulated one is gathered in two narrow fibers. It seems that the pole figures in [21] were produced using the convention where the y axis is parallel to one of x_1, x_2 or x_3 axes, while here the convention where the x axis is parallel to one of x_1, x_2 or x_3 axes is used. For discussion of HCP conventions in use see the Appendix in [6] or the Appendix in [42]. Due to different choice of conventions the $\{11\bar{2}0\}$ pole figures presented here (in Fig. 4) should be compared with $\{10\bar{1}0\}$ pole figures in [21]. The authors of the cited paper managed to simulate
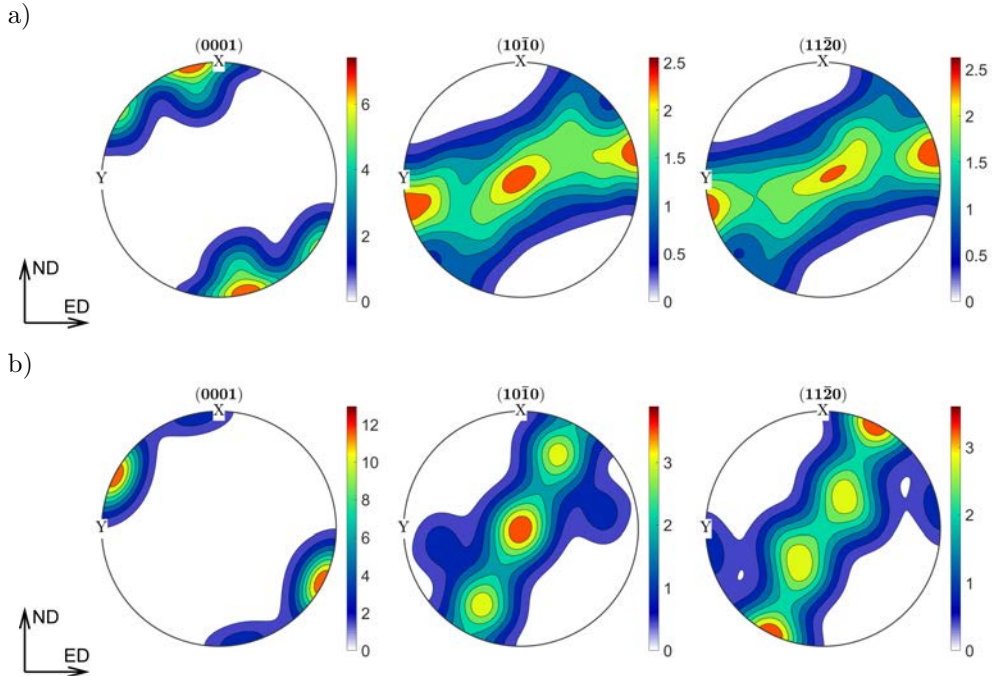
a)

b)

FIG. 4. $\{0001\}$, $\{10\bar{1}0\}$ and $\{11\bar{2}0\}$ pole figures plotted for the texture: a) initially supplied in the simulation, b) after one ECAP pass. The texture has been plotted using the MTEX software [47].

texture evolution such that their PFs were more in line with the experimental data, but one should note that:

- the authors of the cited paper pointed out that the modeling results are very sensitive to the initial texture. They used experimentally obtained texture as the initial one in the simulation. There is no doubt that such texture represents the initial experimental texture better than the texture generated here,

- the cited paper presents *fitting* rather than prediction since the parameters of the model were chosen to obtain the texture similar to the experimental one. Here, the parameters were identified by fitting the stress-strain curves obtained in simple mechanical tests.

Bearing this in mind, one can state that reasonably good ECAP texture *prediction* is done using the VPSC model in the present paper.

3.2. Rotary swaging

Since the RS experiment reported in [35] was performed for an AZ31B rod, it was simulated using the parameters established in [7]. For convenience, the pa-

rameters are given in Table 2. They were established for AZ31B rods compressed at changing loading paths. Similarly as in [8], the parameter optimization was done using the evolutionary algorithm. Rotary swaging results are presented only up to 1.45 strain since in [35] the authors concluded that at 1.90 strain the dynamic recrystallization can have a decisive influence on the resulting texture and such phenomenon is not considered in the model applied here. The predicted texture in the form of inverse pole figures (IPFs) is shown in Fig. 5. The predicted IPF after $\eta = 0.54$ agrees very well with experimental data presented in Fig. 5 of [35]. As concerns larger strain, the prediction is also satisfactory,

Table 2. The parameters of the hardening model for AZ31B extruded rods [7].

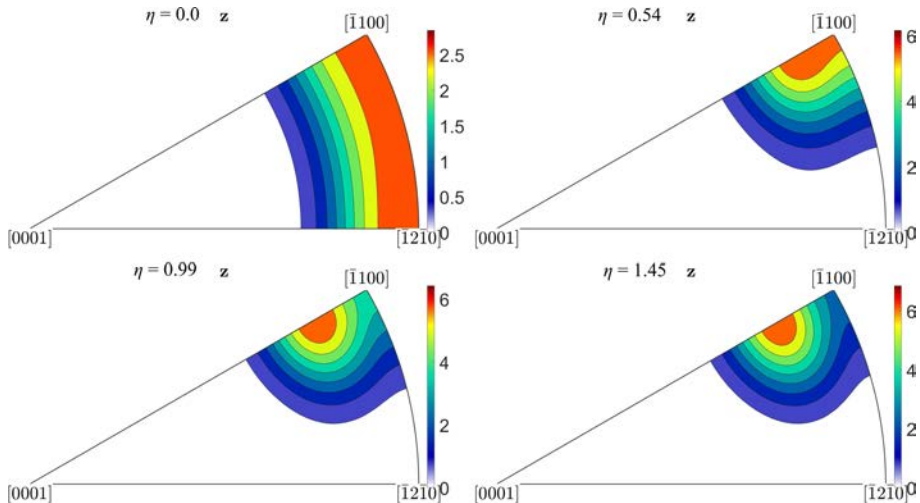| System	Interaction	τ_{c0} [MPa]	h_0 [MPa]	β	τ_{sat}/f_{sat} [MPa]/–	μ –	q prism.	q basal twin	q pyr. II
prism.	slip-slip	32.42	422.04	1.0	132.03	0.82	1.42	1.37	1.6
	slip-twin	—	1.22	—	1.32	—		1.5	
basal	slip-slip	8.7	502.04	1.0	114.8	1.15	1.08	1.33	1.25
	slip-twin	—	1.45	—	1.39	—		1.45	
pyr. II	slip-slip	113.67	1813.53	1.0	137.67	1.36	1.4	1.79	1.51
	slip-twin	—	1.23	—	1.06	—		1.67	
twin	twin-slip	—	94.0	1.0	—	—	1.14	1.46	1.37
	twin-twin	45.33	0.55141	—	0.58	0.62		1.34	

FIG. 5. Inverse pole figures of the wire axis direction obtained in the simulation of rotary swaging after various amounts of strain ($\eta = 0$ means the initially supplied texture). The texture has been plotted using the MTEX software [47].

although minor deviation in the form of a slight shift of the predicted maximum towards the [0001] pole is present. The slip system activities are shown in Fig. 6. One can see that according to the simulation, the prismatic slip was the most active, while considerable portion of strain was also accommodated by pyramidal II ⟨c + a⟩ slip. Twinning was not activated.
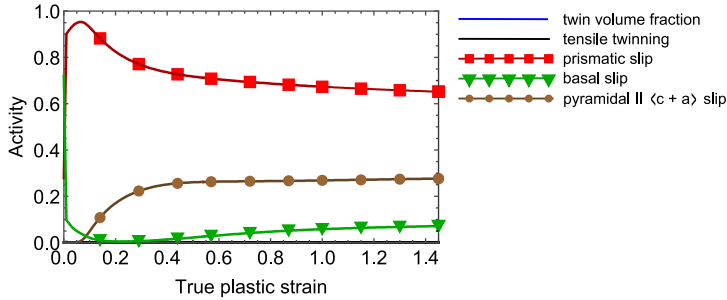

FIG. 6. Slip and twinning system activities in the simulation of rotary swaging.

4. DISCUSSION

To investigate the influence of the initial texture, another simulation of single pass ECAP with same material parameters as in Subsec. 3.1 but with initial random texture was carried out. Figure 7 presents the slip and twinning systems activities, and Fig. 8 presents the resulting texture. The predicted slip and twinning activities are considerably affected by changing the initial texture. The most important differences are the increased activities of the pyramidal and prismatic slips and diminished activity of the basal one. The activity of twinning is similar. As a result, the texture is no longer in agreement with experimental data presented in Fig. 2 of [21]. In principle, the (0001) maximum close to ED moves closer to ND, and the smaller local (0001) maximum moves from ND
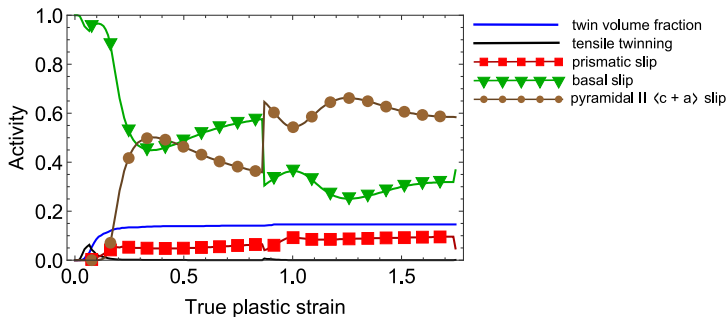

FIG. 7. Slip and twinning system activities in the simulation of one ECAP pass simulated using the initial random texture.
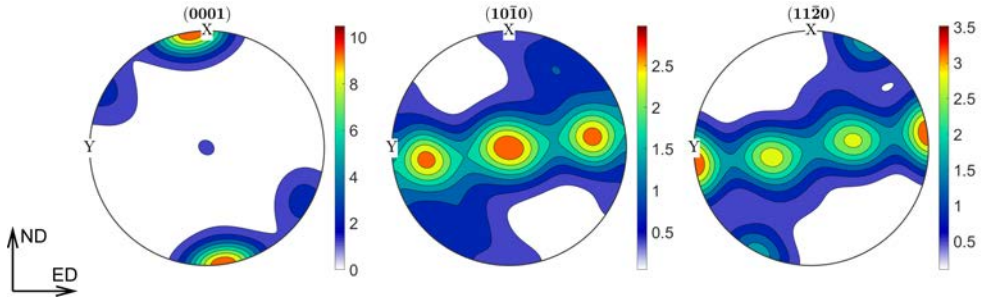
FIG. 8. {0001}, {10$\bar{1}$0} and {11$\bar{2}$0} pole figures plotted for the texture after one ECAP pass *simulated using the initial random texture.* The texture has been plotted using the MTEX software [47].

to ED. This change can also be clearly seen in {10$\bar{1}$0} and {11$\bar{2}$0} pole figures. To conclude, one can confirm the statement of [21] that the initial texture has a very strong influence on the resulting texture.

To show the influence of CP parameters on the resulting texture prediction, two additional simulations were performed. The only difference with respect to the results presented in Sec. 3 was a mutual exchange of the CP parameters, that is the ECAP was now simulated with the parameters established for the rod and the RS was simulated with the parameters established for the sheet. The texture predicted for the ECAP using the rod parameters is presented in Fig. 9. One can see that the agreement with experimental texture presented in Fig. 2b in [21] is still satisfactory. The texture predicted for RS with the sheet parameters with $\eta = 1.45$ is shown in Fig. 10. It can be clearly seen that the prediction is no longer correct. Activities of systems are not presented here due to limited space, but it can be said that such a texture evolution is the result of deformation mainly by the pyramidal II $\langle c + a \rangle$ slip. This is easily understandable when one compares $\tau_{c,0}$ of this system for both materials, see Tables 1 and 2. One can wonder why the ECAP texture is not so much affected
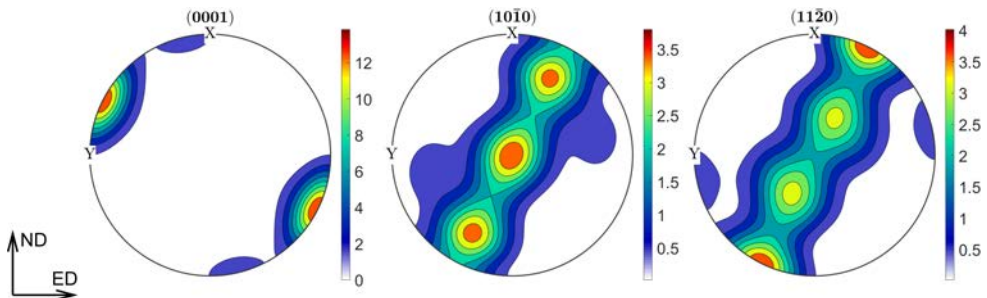

FIG. 9. {0001}, {10$\bar{1}$0} and {11$\bar{2}$0} pole figures plotted for the texture after one ECAP pass *simulated using the parameters established for AZ31B rod (Table 2).* The texture has been plotted using the MTEX software [47].
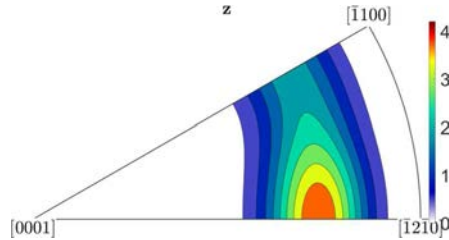
FIG. 10. Inverse pole figures of the wire axis direction obtained in the simulation of rotary swaging after applied strain $\eta = 1.45$ *using the parameters established for AZ31B sheet (Table 1)*. The texture has been plotted using the MTEX software [47].

by the change of CP parameters. The point is that in the case of ECAP, the main plastic deformation carrier is the basal slip with some aid provided by the pyramidal slip, see Fig. 4. The rod parameters specify much lower CRSS for the prismatic slip and somewhat higher for the basal slip. The result is that in the first simple shear there is a drop in basal slip activity compensated by the prismatic slip. However, in the second simple shear the final activity of the systems is very similar to the simulation with sheet parameters, which suggests that the saturated CRSS are similar. This is why the texture changes only moderately and the overall result is still consistent with the measurements.

Besides strong texture evolution, SPD processes can lead to considerable grain refinement. While this is an important issue, the two-scale self-consistent crystal plasticity model applied here cannot provide any information about phenomena on the scale lower than a grain scale. In addition, Mg and its alloys possess very low dynamic recrystallization temperature. Dynamic recrystallization (DRX) in Mg leads to $30°$ rotation around the "c" axis [21, 48, 49]. Gu and Toth [21] concluded that during one ECAP pass, DRX was active but the resulting texture is the B-fiber, of which the fibre axis is the "c" axis. Therefore the rotation associated with DRX does not influence the resulting texture. Due to the activation of the DRX, the 3SCP model developed for FCC metals [50] and applied later for titanium [42] and stainless steel [51] is probably not able to capture grain refinement in AZ31B. In the case of this material, such phenomenon should be treated with other models, such as, e.g., cellular automata [52].

5. SUMMARY AND CONCLUSIONS

The paper presents the simulations of texture evolution in two SPD processes, namely the ECAP and rotary swaging. The parameters of the model were calibrated in previous studies, thus all the results presented here are pure predictions. Both the resulting textures and the slip and twinning system ac-

tivities leading to their development are shown. This provides the insight into the microstructural mechanisms active in both processes. Based on the obtained results, the following conclusions can be drawn:

- the initial texture has non-negligible effect upon the final texture in ECAP,
- the crystal plasticity model can be successfully applied to simulate the rotary swaging process applied to AZ31b Mg alloy; note that, to the best of author's knowledge, this is a first study presenting the crystal plasticity simulation of rotary swaging,
- crystal plasticity model parameters established by matching stress-strain curves with the help of an evolutionary algorithm [7, 8] can be applied to predict texture evolution in material subjected to severe plastic deformation and provide good agreement with experimental data.

Acknowledgement

References

1. Fu H., Ge B., Xin Y., Wu R., Fernandez C., Huang J., Peng Q., Achieving high strength and ductility in magnesium alloys via densely hierarchical double contraction nanotwins, *Nano letters*, **17**(10): 6117–6124, 2017, doi: 10.1021/acs.nanolett.7b02641.

2. Agnew S.R., Yoo M.H., Tomé C.N., Application of texture simulation to understanding mechanical behavior of Mg and solid solution alloys containing Li or Y, *Acta Materialia*, **49**(20): 4277–4289, 2001, doi: 10.1016/S1359-6454(01)00297-X.

3. Clausen B., Tomé C.N., Brown D.W., Agnew S.R., Reorientation and stress relaxation due to twinning: Modeling and experimental characterization for Mg, *Acta Materialia*, **56**(11): 2456–2468, 2008, doi: 10.1016/j.actamat.2008.01.057.

4. Ebeling T., Hartig Ch., Laser T., Bormann R., Material law parameter determination of magnesium alloys, *Materials Science and Engineering: A*, **527**(1–2): 272–280, 2009, doi: 10.1016/j.msea.2009.07.072.

5. Herrera-Solaz V., Llorca J., Dogan E., Karaman I., Segurado J., An inverse optimization strategy to determine single crystal mechanical behavior from polycrystal tests: Application to AZ31 Mg alloy, *International Journal of Plasticity*, **57**: 1–15, 2014, doi: 10.1016/j.ijplas.2014.02.001.

6. Frydrych K., *Modelling of microstructure evolution of high specific strength metals subjected to severe plastic deformation processes* [in Polish: *Modelowanie ewolucji mikrostruktury metali o wysokiej wytrzymałości właściwej w procesach intensywnej deformacji plastycznej*], Ph.D. thesis, Institute of Fundamental Technological Research, Polish Academy of Sciences, Warsaw, Poland, 2017, doi: 10.13140/RG.2.2.32354.56008.

7. FRYDRYCH K., MAJ M., URBAŃSKI L., KOWALCZYK-GAJEWSKA K., Twinning-induced anisotropy of mechanical response of AZ31B extruded rods, *Materials Science and Engineering: A*, **771**: 138610, 2020, doi: 10.1016/j.msea.2019.138610.

8. FRYDRYCH K., LIBURA T., KOWALEWSKI Z., MAJ M., KOWALCZYK-GAJEWSKA K., On the role of slip, twinning and detwinning in magnesium alloy AZ31B sheet, *Materials Science and Engineering A*, **813**: 141152, 2021, doi: 10.1016/j.msea.2021.141152.

9. SEGAL V.M., *Methods of stress-strain analysis in metalforming*, Sc.D. Thesis, Physical-Technical Institute Academy of Sciences of Belorus, Minsk, USSR, 1979.

10. SEGAL V.M., Materials processing by simple shear, *Materials Science and Engineering: A*, **197**(2): 157–164, 1995, doi: 10.1016/0921-5093(95)09705-8.

11. EDDAHBI M., DEL VALLE J.A., PÉEREZ-PRADO M.T., RUANO O.A., Comparison of the microstructure and thermal stability of an AZ31 alloy processed by ECAP and large strain hot rolling, *Materials Science and Engineering: A*, **410–411**: 308–311, 2005, doi: 10.1016/j.msea.2005.08.081.

12. AGNEW S.R., MEHROTRA P., LILLO T.M., STOICA G.M., LIAW, P.K., Texture evolution of five wrought magnesium alloys during route A equal channel angular extrusion: Experiments and simulations, *Acta Materialia*, **53**(11): 3135–3146, 2005, doi: 10.1016/j.actamat.2005.02.019.

13. AGNEW S.R., MEHROTRA P., LILLO T.M., STOICA G.M., LIAW P.K., Crystallographic texture evolution of three wrought magnesium alloys during equal channel angular extrusion, *Materials Science and Engineering: A*, **408**(1–2): 72–78, 2005, doi: 10.1016/j.msea.2005.07.052.

14. DEL VALLE J.A., CARREÑO F., RUANO O.A., Influence of texture and grain size on work hardening and ductility in magnesium-based alloys processed by ECAP and rolling, *Acta Materialia*, **54**(16): 4247–4259, 2006, doi: 10.1016/j.actamat.2006.05.018.

15. WU L., STOICA G.M., LIAO H.-H, AGNEW S.R., PAYZANT E.A., WANG G., FIELDEN D., CHEN L., LIAW P.K., Fatigue-property enhancement of magnesium alloy, AZ31B, through equal-channel-angular pressing, *Metallurgical and Materials Transactions A*, **38**(13): 2283–2289, 2007, doi: 10.1007/s11661-007-9123-8.

16. BEAUSIR B., SUWAS S., TÓTH L.S., NEALE K.W., FUNDENBERGER J.-J., Analysis of texture evolution in magnesium during equal channel angular extrusion, *Acta Materialia*, **56**(2): 200–214, 2008, doi: 10.1016/j.actamat.2007.09.032.

17. AL-MAHARBI M., KARAMAN I., BEYERLEIN I.J., FOLEY D., HARTWIG K.T., KECSKES L.J., MATHAUDHU S.N., Microstructure, crystallographic texture, and plastic anisotropy evolution in an Mg alloy during equal channel angular extrusion processing, *Materials Science and Engineering: A*, **528**(25–26): 7616–7627, 2011, doi: 10.1016/j.msea.2011.06.043.

18. FIGUEIREDO R.B., LANGDON T.G., Grain refinement and mechanical behavior of a magnesium alloy processed by ECAP, *Journal of Materials Science*, **45**(17): 4827– 4836, 2010, doi: 10.1007/s10853-010-4589-y.

19. OSTAPOVETS, A., ŠEDÁ P., JÄGER A., LEJČEK P., New misorientation scheme for a viscoplastic self-consistent model: Equal channel angular pressing of magnesium single crystals, *International Journal of Plasticity*, **29**: 1–12, 2012, doi: 10.1016/ j.ijplas.2011.07.006.

20. Seipp S., Wagner M.F.-X., Hockauf K., Schneider I., Meyer L.W., Hockauf M., Microstructure, crystallographic texture and mechanical properties of the magnesium alloy AZ31B after different routes of thermo-mechanical processing, *International Journal of Plasticity*, **35**: 155–166, 2012, doi: 10.1016/j.ijplas.2012.03.007.

21. Gu C.F., Tóth L.S., Field D., Fundenberger J.J., Zhang Y.D., Room temperature equal-channel angular pressing of a magnesium alloy, *Acta Materialia*, **61**(8): 3027–3036, 2013, doi: 10.1016/j.actamat.2013.01.063.

22. Karami M., Mahmudi R., The microstructural, textural, and mechanical properties of extruded and equal channel angularly pressed Mg-Li-Zn alloys, *Metallurgical and Materials Transactions A*, **44**(8): 3934–3946, 2013, doi: 10.1007/s11661-013-1699-6.

23. Biswas S., Singh D.S., Beausir B., Tóth L.S., Suwas S., Thermal response on the microstructure and texture of ECAP and cold-rolled pure magnesium, *Metallurgical and Materials Transactions A*, **46**(6): 2598–2613, 2015, doi: 10.1007/s11661-015- 2846-z.

24. Gzyl M., Rosochowski A., Pesci, R., Olejnik L., Yakushina, E., Wood P., Mechanical properties and microstructure of AZ31B magnesium alloy processed by I-ECAP, *Metallurgical and Materials Transactions A*, **45**(3): 1609–1620, 2014, doi: 10.1007/s11661-013-2094-z.

25. Gzyl M., Rosochowski A., Boczkal S., Qarni M.J., The origin of fracture in the I-ECAP of AZ31B magnesium alloy, *Metallurgical and Materials Transactions A*, **46**(11): 5275–5284, 2015, doi: 10.1007/s11661-015-3069-z.

26. Ostapovets A., Molnár P., Jäger A., Visco-plastic self-consistent modelling of a grain boundary misorientation distribution after equal-channel angular pressing in an AZ31 magnesium alloy, *Journal of Materials Science*, **48**(5): 2123– 2134, 2013, doi: 10.1007/s10853-012-6987-9.

27. Hutchinson J.W., Bounds and self-consistent estimates for creep of polycrystalline materials, *Proceedings of the Royal Society of London A*, **348**(1652): 101–127, 1976, doi: 10.1098/rspa.1976.0027.

28. Molinari A., Canova G.R., Ahzi S., A self-consistent approach of the large deformation polycrystal visco-plasticity, *Acta Metallurgica*, **35**(12): 2983–2994, 1987, doi: 10.1016/0001-6160(87)90297-5.

29. Lebensohn R.A., Tomé C.N., A self-consistent anisotropic approach for the simulation of plastic deformation and texture development of polycrystals: Application to zirconium alloys, *Acta Metallurgica et Materialia*, **41**(9): 2611– 2624, 1993, doi: 10.1016/0956-7151(93)90130-K.

30. Frydrych K., Kowalczyk-Gajewska K., Grain refinement in the equal channel angular pressing process: simulations using the crystal plasticity finite element method, *Modelling and Simulation in Materials Science and Engineering*, **26**(6): 065015, 2018, doi: 10.1088/1361-651X/aad46d.

31. Frydrych K., Kowalczyk-Gajewska K., Prakash A., On solution mapping and remeshing in crystal plasticity finite element simulations: application to equal channel angular pressing, *Modelling and Simulation in Materials Science and Engineering*, **27**(7): 075001, 2019, doi: 10.1088/1361- 651X/ab28e3.

32. Minakowski P., Fluid model of crystal plasticity: numerical simulations of 2-turn equal channel angular extrusion, *Technische Mechanik*, **34**(3–4): 213–221, 2014, doi: 10.24352/UB.OVGU-2017-063.

33. RONG L., NIE Z., ZUO T., 3D finite element modeling of cogging-down rotary swaging of pure magnesium square billet – revealing the effect of high-frequency pulse stroking, *Materials Science and Engineering A*, **464**(1–2): 28–37, 2007, doi: 10.1016/j.msea.2007.01.086.

34. MOUMI E., ISHKINA S., KUHFUSS B., HOCHRAINER T., STRUSS A., HUNKEL M., 2D-simulation of material flow during infeed rotary swaging using finite element method, *Procedia Engineering*, **81**: 2342–2347, 2014, doi: 10.1016/j.proeng.2014.10.331.

35. KNAUER E., FREUDENBERGER J., MARR T., KAUFFMANN A., SCHULTZ L., Grain refinement and deformation mechanisms in room temperature severe plastic deformed Mg-AZ31, *Metals*, **3**(3): 283–297, 2013, doi: 10.3390/met3030283.

36. GAN W.M., HUANG Y.D., WANG R., WANG G.F., SRINIVASAN A., BROKMEIER H.-G., SCHELL N., KAINER K. U., HORT N., Microstructures and mechanical properties of pure Mg processed by rotary swaging, *Materials and Design*, **63**: 83–88, 2014, doi: 10.1016/j.matdes.2014.05.057.

37. MARTYNENKO N.S., LUK'YANOVA E.A., MOROZOV M.M., YUSUPOV V.S., DOBATKIN S.V., ESTRIN Y.Z., A study of the structure, mechanical properties and corrosion resistance of magnesium alloy WE43 after rotary swaging, *Metal Science and Heat Treatment*, **60**(3–4): 253–258, 2018, doi: 10.1007/s11041-018-0269-3.

38. TOMÉ C.N., LEBENSOHN R.A., *Manual for Code Visco-Plastic Self-Consistent (VPSC)*, Version 7b, Tech. rep., Los Alamos National Laboratory, 2007, https://public.lanl.gov/lebenso/VPSC7c_manual.pdf.

39. KOWALCZYK-GAJEWSKA K., Modelling of texture evolution in metals accounting for lattice reorientation due to twinning, *European Journal of Mechanics – A/Solids*, **29**(1): 28–41, 2010, doi: 10.1016/j.euromechsol.2009.07.002.

40. KOWALCZYK-GAJEWSKA K., Micromechanical modelling of metals and alloys of high specific strength, *IFTR Reports 1/2011*, pp. 1–299, 2011.

41. KOWALCZYK-GAJEWSKA K., SZTWIERTNIA K., KAWAŁKO, J., WIERZBANOWSKI K., WROŃSKI K., FRYDRYCH K., STUPKIEWICZ S., PETRYK H., Texture evolution in titanium on complex deformation paths: Experiment and modelling, *Materials Science and Engineering: A*, **637**: 251–263, 2015, doi: 10.1016/j.msea.2015.04.040.

42. FRYDRYCH K., KOWALCZYK-GAJEWSKA K., Microstructure evolution in cold-rolled pure titanium: modeling by the three-scale crystal plasticity approach accounting for twinning, *Metallurgical and Materials Transactions A*, **49**(8): 3610–3623, 2018, doi: 10.1007/s11661-018-4676-2.

43. ASARO R.J., NEEDLEMAN A., Overview no 42 Texture development and strain hardening in rate dependent polycrystals, *Acta Metallurgica*, **33**(6): 923–953, 1985, doi: 10.1016/0001-6160(85)90188-9.

44. VAN HOUTTE P., Simulation of the rolling texture and shear texture of brass by the Taylor theory adapted for mechanical twinning, *Acta Metallurgica*, **26**(4): 591–604, 1978, doi: 10.1016/0001-6160(78)90111-6.

45. TOMÉ C.N., LEBENSOHN R.A., KOCKS U.F., A model for texture development dominated by deformation twinning: application to zirconium alloy, *Acta Metallurgica et Materialia*, **39**(11): 2667–2680, 1991, doi: 10.1016/0956-7151(91)90083-D.

46. SALEM A.A., KALIDINDI S.R., SEMIATIN S.L., Strain hardening due to deformation twinning in α-titanium: Constitutive relations and crystal plasticity modeling, *Acta Materialia*, **53**(12): 3495–3502, 2005, doi: 10.1016/j.actamat.2005.04.014.

47. HIELSCHER R., SCHAEBEN H., A novel pole figure inversion method: specification of the MTEX algorithm, *Journal of Applied Crystallography*, **41**(6): 1024–1037, 2008, doi: 10.1107/S0021889808030112.

48. BISWAS S., BROKMEIER H.-G., FUNDENBERGER J.-J., SUWAS S., Role of deformation temperature on the evolution and heterogeneity of texture during equal channel angular pressing of magnesium, *Materials Characterization*, **102**: 98–102, 2015, doi: 10.1016/j.matchar.2015.02.021.

49. KRYWOPUSK N.M., KECSKES L.J., WEIHS T.P., Microstructural characterization of pure Mg and AZ31B processed by ECAE, *Materials Characterization*, **158**: 109950, 2019, doi.org/10.1016/j.matchar.2019.109950.

50. FRYDRYCH K., KOWALCZYK-GAJEWSKA K., A three-scale crystal plasticity model accounting for grain refinement in FCC metals subjected to severe plastic deformations, *Materials Science and Engineering: A*, **658**: 490–502, 2016, doi: 10.1016/j.msea.2016.01.101.

51. FRYDRYCH K., Simulations of grain refinement in various steels using the three-scale crystal plasticity model, *Metallurgical and Materials Transactions A*, **50**(10): 4913–4919, 2019, doi: 10.1007/s11661-019-05373-z.

52. GZYL M.Z., ROSOCHOWSKI A., MILENIN A., OLEJNIK L., Modelling microstructure evolution during equal channel angular pressing of magnesium alloys using cellular automata finite element method, *Computer Methods in Materials Science*, **13**(2): 357–363, 2013, https://strathprints.strath.ac.uk/id/eprint/43378.